Cell Chemical Biology

In vivo drug discovery for increasing incretin-expressing cells identifies DYRK inhibitors that reinforce the enteroendocrine system

Graphical abstract

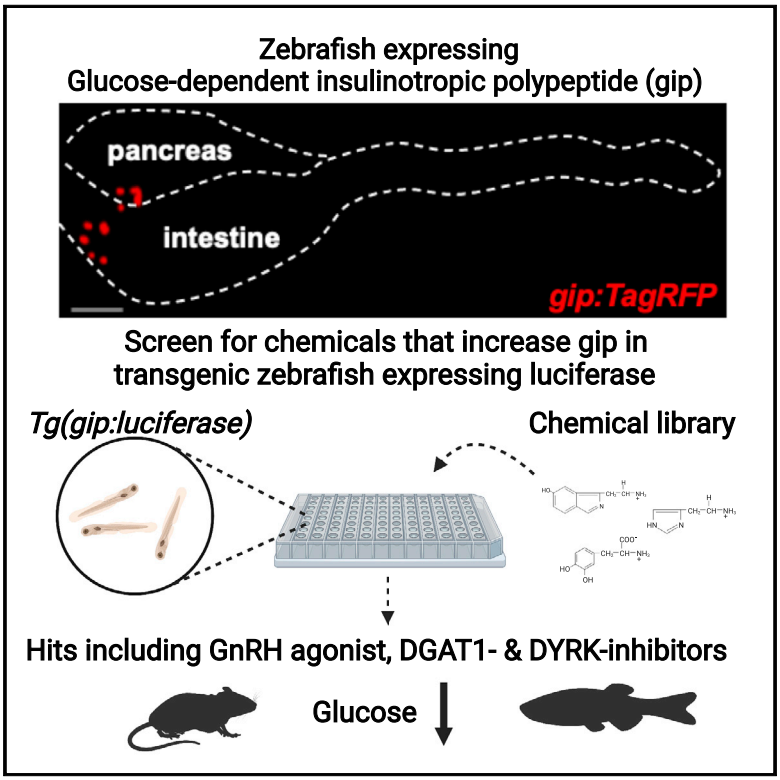

Highlights

- *In vivo* screen identifies small molecules that increase the number of incretin$^+$ cells
- A GnRH agonist and DGAT1 and DYRK inhibitors boost differentiation of incretin$^+$ cells
- DYRK1A/B and downstream NFATC4 regulate the differentiation of incretin$^+$ cells
- DYRK inhibitors improve glucose control in both zebrafish and diabetic mice

Authors

Lianhe Chu, Michishige Terasaki, Charlotte L. Mattsson, ..., Nils Wierup, Rohit N. Kulkarni, Olov Andersson

Correspondence

olov.andersson@ki.se

In brief

Analogs of the incretin hormones Gip and Glp-1 are typically used to treat diabetes. To identify factors directly increasing the number of incretin-expressing cells, Chu et al. establish a zebrafish screen and identify multiple hits, including DYRK inhibitors that increase incretins and improve glucose control in zebrafish and diabetic mice.

Chu et al., 2022, Cell Chemical Biology *29*, 1368–1380
September 15, 2022
https://doi.org/10.1016/j.chembiol.2022.08.001

CellPress

CellPress
OPEN ACCESS

Cell Chemical Biology

Article

In vivo drug discovery for increasing incretin-expressing cells identifies DYRK inhibitors that reinforce the enteroendocrine system

Lianhe Chu,[1,7] Michishige Terasaki,[1,7] Charlotte L. Mattsson,[1,7] Romain Teinturier,[1] Jérémie Charbord,[1] Ercument Dirice,[2,6] Ka-Cheuk Liu,[1] Michael G. Miskelly,[3] Qiao Zhou,[4] Nils Wierup,[3] Rohit N. Kulkarni,[2,5] and Olov Andersson[1,8,*]

[1]Department of Cell and Molecular Biology, Karolinska Institutet, Stockholm, Sweden
[2]Islet Cell and Regenerative Biology, Joslin Diabetes Center, Department of Medicine, Harvard Medical School, Boston, MA 02215, USA
[3]Department of Clinical Sciences, Lund University Diabetes Centre, Malmö 20502, Sweden
[4]Division of Regenerative Medicine & Ansary Stem Cell Institute, Department of Medicine, Weill Cornell Medicine, 1300 York Avenue, New York, NY 10065, USA
[5]Harvard Stem Cell Institute, Boston, MA 02215, USA
[6]Present address: Department of Pharmacology, New York Medical College, Valhalla, NY, USA
[7]These authors contributed equally
[8]Lead contact
*Correspondence: olov.andersson@ki.se
https://doi.org/10.1016/j.chembiol.2022.08.001

SUMMARY

Analogs of the incretin hormones Gip and Glp-1 are used to treat type 2 diabetes and obesity. Findings in experimental models suggest that manipulating several hormones simultaneously may be more effective. To identify small molecules that increase the number of incretin-expressing cells, we established a high-throughput *in vivo* chemical screen by using the *gip* promoter to drive the expression of luciferase in zebrafish. All hits increased the numbers of neurogenin 3-expressing enteroendocrine progenitors, Gip-expressing K-cells, and Glp-1-expressing L-cells. One of the hits, a dual-specificity tyrosine phosphorylation-regulated kinase (DYRK) inhibitor, additionally decreased glucose levels in both larval and juvenile fish. Knock-down experiments indicated that *nfatc4*, a downstream mediator of DYRKs, regulates incretin^{+} cell number in zebrafish, and that *Dyrk1b* regulates Glp-1 expression in an enteroendocrine cell line. DYRK inhibition also increased the number of incretin-expressing cells in diabetic mice, suggesting a conserved reinforcement of the enteroendocrine system, with possible implications for diabetes.

INTRODUCTION

Hormones released from the gastrointestinal tract have important roles in metabolism, by modulating satiety, gut motility, insulin secretion, and plasma glucose levels (Gribble and Reimann, 2019). Of particular relevance to diabetes, the incretins are hormones secreted upon food intake and enhance glucose-stimulated insulin secretion, thereby decreasing plasma glucose levels (Boer and Holst, 2020). The major incretins are the glucagon-like peptide-1 (GLP-1) and glucose-dependent insulinotropic polypeptide (GIP); GLP-1 is secreted predominantly by the L-cells, and GIP by the K-cells, of the intestine. To date, there has been extensive research on GLP-1, resulting in efficient GLP-1-based therapeutics for diabetes and obesity, whereas no therapeutics has been developed based on solely GIP, although inhibitors of the enzyme degrading GLP-1 and GIP (DPP4) affect both hormones (Boer and Holst, 2020). The last few years, several dual, or even triple, agonists of GLP-1, GIP, glucagon, or estrogen have emerged as promising agents with synergistic effects on metabolic readouts (Baggio and Drucker, 2021; Brandt et al., 2018; Holst and Rosenkilde, 2020). Moreover, recent findings suggest that GIP has a more pivotal role in glucose homeostasis than previously thought, especially in humans (Finan et al., 2016; Gasbjerg et al., 2019). In addition to increasing insulin secretion, GIP has been shown to act on the hypothalamus to regulate food intake and thereby obesity (Adriaenssens et al., 2019). Pathophysiologically, GIP secretion and GIP sensitization are significantly impaired in patients with type 2 diabetes (Xu et al., 2007) or chronic GIP agonism (Killion et al., 2020), and this impairment decreases insulin secretion. Thus, an enhanced capacity of GIP production or secretion seems beneficial in pre-diabetes and type 2 diabetes, or perhaps more efficiently, a simultaneous boost in the level of several enteroendocrine hormones to reinforce the gut's response to food intake.

The zebrafish model is ideal for *in vivo* drug discovery, combining the high throughput of *in vitro* screens with the physiological complexity and relevance of animal studies (Lam and

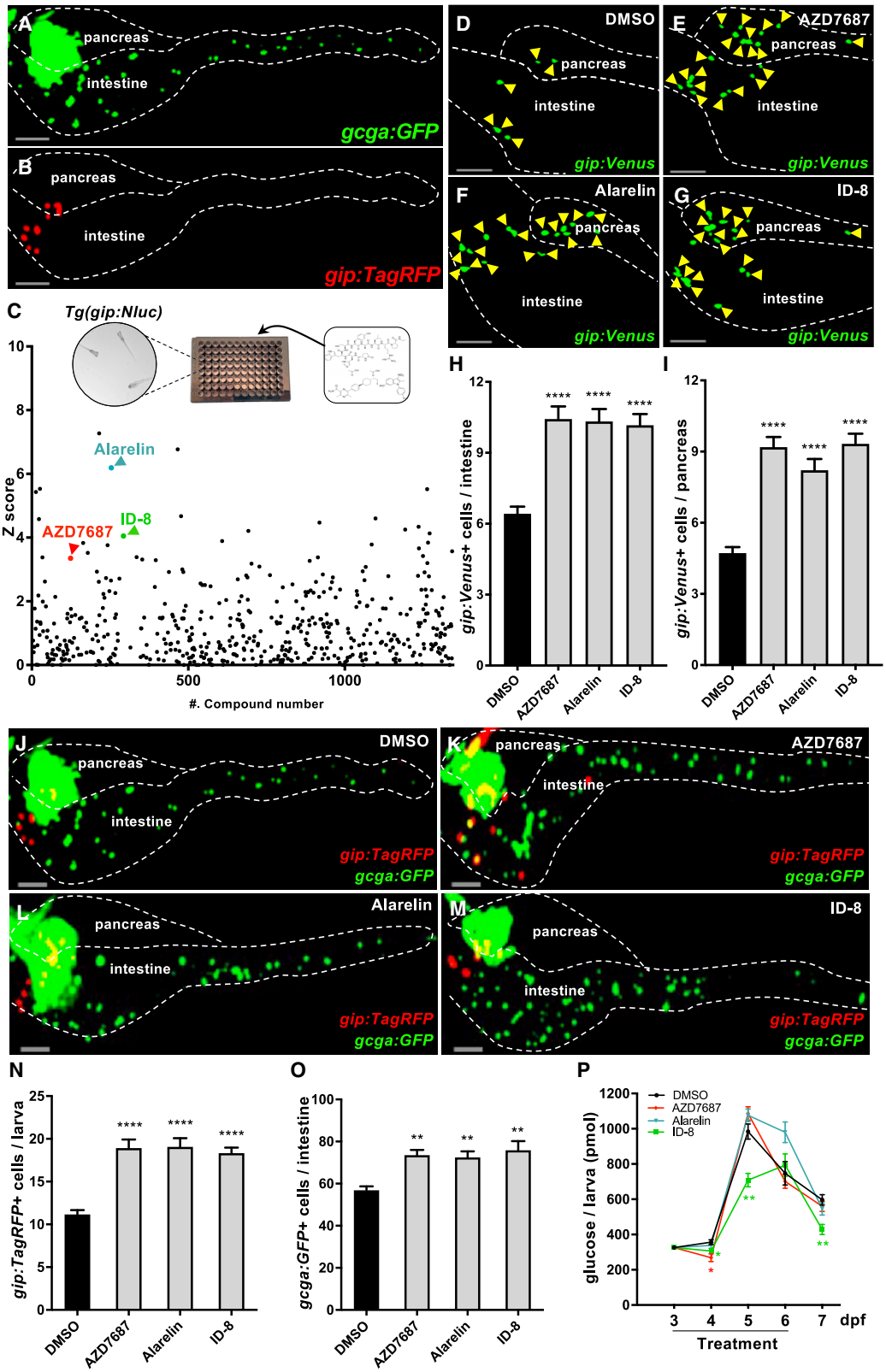

(legend on next page)

Peterson, 2019). Moreover, the zebrafish has been extensively used for studying development and function of the pancreas (Kimmel and Meyer, 2016) and liver (Pham et al., 2017), and several chemical or genetic screens have been performed for improving the function of these organs in metabolic control (Andersson et al., 2012; Charbord et al., 2021; Lu et al., 2016; Massoz et al., 2021; Singh and Ninov, 2018; Yang et al., 2020). However, with regard to the enteroendocrine system in zebrafish, despite several thorough studies of development and function (Crosnier et al., 2005; Flasse et al., 2013; Ng et al., 2005; Reuter et al., 2022; Ye et al., 2019) and incretins (Graham et al., 2018; Musson et al., 2010), chemical screening opportunities remain unexplored (Gut et al., 2017). Here, we made use of the advantageous features of the zebrafish model and performed a high-throughput screen for *gip*-expression and found that DYRK inhibitors stimulate the formation of several enteroendocrine cell types to reinforce the enteroendocrine system in both zebrafish and mice.

RESULTS

In vivo chemical screening identified small molecules increasing the number of incretin-expressing cells in zebrafish

We aimed to perform a high-throughput screen for small molecules increasing the number of incretin-expressing cells using luminescence in whole zebrafish larvae. However, transgenic zebrafish expressing GFP under the control of the *proglucagon* promoter, *Tg*(*gcga*:*GFP*), mainly labeled α-cells in the pancreas (Figure 1A), rendering the *proglucagon* promoter unusable for high-throughput screening of incretin-producing cells using luciferase, which reports the total expression in the whole zebrafish. Therefore, we cloned the proximal promoter of *gip* and used it to drive the expression of TagRFP, *Tg*(*gip*:*TagRFP*), which specifically marked K-cells in the upper intestine and a few cells in the pancreas (and nowhere else in the whole zebrafish) (Figure 1B), in line with previous findings (Musson et al., 2009). To enable the high-throughput screening of chemicals, we generated another transgenic zebrafish line expressing nano-luciferase under the control of the *gip* promoter, *Tg*(*gip*:*Nluc*), which was used to screen 1,303 small molecules with the aim of identifying small molecules that increased the number of *gip*-expressing K-cells in the gut (Figure 1C). We treated the larvae from 3 to 6 days post fertilization with the small molecules in 96-well plates with three larvae per well. After rescreening 95 primary hits with a Z-score of greater than 2 in 4 additional independent wells, we confirmed 3 small molecules that most often (i.e., gave a Z-score of >2 in at least 3 of the wells) increased the luminescence signal generated in *Tg*(*gip*:*Nluc*), i.e., Alarelin, AZD7687, and ID-8 (Figure 1C). Alarelin is an agonist of the gonadotropin-releasing hormone receptor, AZD7687 is an inhibitor of diacylglycerol acyltransferase 1, and ID-8 is an inhibitor of dual-specificity tyrosine phosphorylation-regulated kinases (DYRKs). All three hits not only increased the overall expression of *gip*, but also increased the number of K-cells in the intestine as well as the *gip*-expressing cells in the pancreas (Figures 1D–1I). We continued by examining whether the identified hits also increased the number of L-cells by quantifying the number of *gcga*:GFP-expressing cells in the intestine [the *Tg(gcga*:*GFP)* was used as a proxy for Glp-1 expression in the absence of antibodies recognizing zebrafish Glp-1, but may also report on Glucagon and Glp-2 expression]. In double transgenic *Tg(gcga*:*GFP)*;*Tg(gip*:*TagRFP)* we found that all three hits increased the number of both L- and K-cells (Figures 1J–1O), without showing much overlapping expression. Next, we examined whether the hits could decrease the glucose levels in the larvae, and found that AZD7687 and ID-8 led to a significant decrease in glucose during the treatment period (Figure 1P). This decrease was not due to an increase in the number of insulin-producing β-cells (Figures S1A–S1C). Thus, we succeeded

Figure 1. *In vivo* chemical screening identified small molecules increasing the number of incretin-expressing cells in zebrafish

(A and B) Representative confocal projections of a 6 days post fertilization (dpf) *Tg*(*gip*:*TagRFP*);*Tg*(*gcga*:*GFP*) larva. The expression of *Tg*(*gcga*:*GFP*) (A) mainly appeared in the pancreatic islet and enteroendocrine cells throughout the gut, whereas *Tg*(*gip*:*TagRFP*) (B) mainly appeared in enteroendocrine cells of upper gut in the intestinal bulb and pancreas. Scale bars, 100 μm.

(C) Top: Schematic depicting the screening for compounds stimulating the expressing of *gip* in whole zebrafish larvae. Three *Tg*(*gip*:*Nluc*) zebrafish larvae at 3 dpf were transferred to each well of 96-well plates. A compound from the MedChemExpress library was added to each well containing 200 μL E3 + PTU solution. At 6 dpf, the luminescence activity was measured. Bottom: Three hits were identified, including AZD7687, Alarelin, and ID-8. Data are shown with calculated Z-score of compounds from the MedChemExpress library. *Tg*(*gip*:*Nluc*) larvae were treated from 3 to 6 dpf with DMSO or one of the 1,303 chemicals. Luminescence activity was measured at 6 dpf and displayed as Z-scores.

(D–I) The hits promote the generation of *gip*-expressing cells both in the intestine and pancreas in zebrafish larvae. (D–G) Representative confocal images of *Tg*(*gip*:*Venus*) larvae treated from 3 to 6 dpf with DMSO (D) or the hits including AZD7687 (E), Alarelin (F), and ID-8 (G). Yellow arrowheads show *gip*:*Venus* positive cells. Scale bars, 50 μm.

(H) Quantification of the number of *gip*:*Venus*-positive cells in the intestine of 6 dpf *Tg*(*gip*:*Venus*) larvae after the treatments in (D–G). n = 40–57 larvae per group. ****p < 0.0001. (I) Quantification of the number of *gip*:*Venus*-positive cells in the pancreas of *Tg*(*gip*:*Venus*) after the treatments in (D–G). n = 38–57 larvae per group. ****p < 0.0001.

(J–O) Hit compounds promotes the generation of K-cells and L-cells in the intestines of zebrafish larvae.

(J–M) Representative confocal projections of *Tg*(*gip*:*TagRFP*); *Tg*(*gcga*:*GFP*) larvae treated from 3 to 6 dpf with DMSO (J), AZD7687 (K), Alarelin (L), or ID-8 (M), displaying *gip*:*TagRFP*-expressing cells in red and *gcga*:*GFP* expressing cells in green. The same larva is displayed with single and merged channels in Figures 1A and 1B and 1J. Scale bars, 100 μm.

(N) Quantification of the total number of K-cells in *Tg*(*gip*:*TagRFP*);*Tg*(*gcga*:*GFP*) larvae after treatment. n = 17–23 larvae per group.

(O) Quantification of the total number of L-cells in the intestines of *Tg*(*gip*:*TagRFP*);*Tg*(*gcga*:*GFP*) larvae after treatment. Since *gcga*:*GFP*-expressing cells were lumped in the islet, we did not quantify the number of these cells in the pancreas. n = 10–12 larvae per group. ****p < 0.0001, **p < 0.01.

(P) Free glucose levels (i.e., glucose that has not been phosphorylated) were measured in wild-type zebrafish larvae treated from 3 to 6 dpf with DMSO, AZD7687, Alarelin, or ID-8. We sampled larvae for free glucose levels in consecutive days from 3 to 7 dpf. Free glucose levels were significantly lower in the larvae treated with ID-8 (green line) than those with DMSO (black line) at 4, 5, and 7 dpf; the only other significance was the AZD7687-treated group at 4 dpf. n = 16 larvae (8 pools of 2 larvae) per data point, **p < 0.01, *p < 0.05. See also Figure S1.

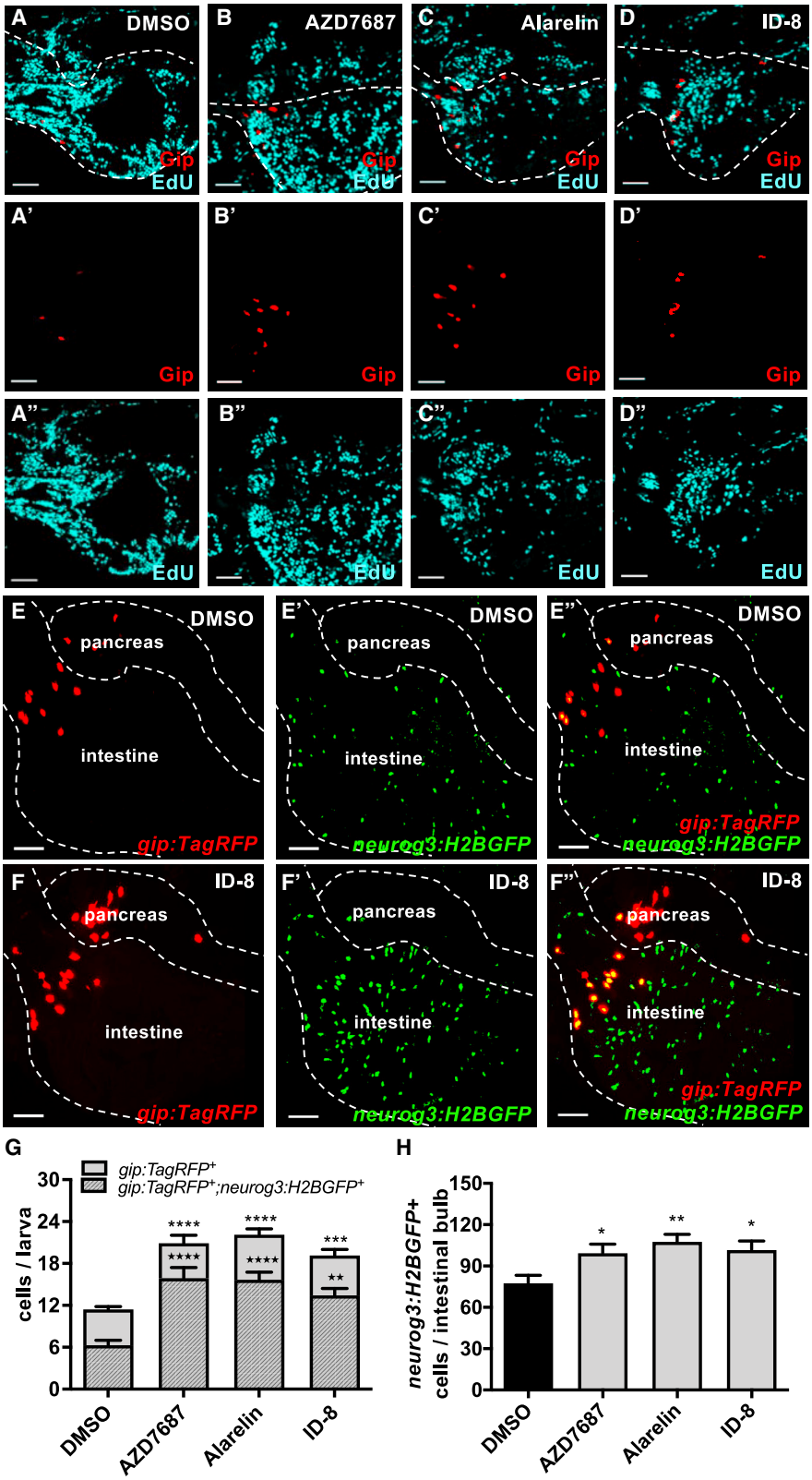

Figure 2. The hits promote neogenesis of K-cells originating from neurog3^{+} progenitor cells

(A–D) No proliferation of K-cells was observed in the intestines after treatment with the hits. Representative confocal projection images of *gip:TagRFP*-expressing cells (in red) and EdU positive cells (in cyan blue) in the intestines of *Tg(gip:TagRFP)* zebrafish larvae treated from 3 to 6 days post fertilization (dpf) with DMSO (A),

(legend continued on next page)

in creating genetic models that allowed us to perform the intended screen and confirmed that the hits not only boosted the expression of *gip*, but also increased the number of K- and L-cells.

The hits promote neogenesis of K-cells originating from neurog3$^+$ progenitor cells

We examined the cellular mechanism behind the increase in K-cells by proliferation and lineage-tracing studies. None of the K-cells in the control or treatment group were labeled by EdU, indicating that the increased number of K-cells was not due to proliferation (Figures 2A–2D), nor did the Gip-expressing cells in the pancreas proliferate (Figures S1D–S1G). Next, we generated a transgenic line stably marking *neurogenin 3*-expressing enteroendocrine progenitors (Jenny et al., 2002) by expressing H2BGFP under the control of its promoter, *Tg*(*neurog3*:*H2BGFP*), and found that all three hits increased the number of K-cells labeled by H2BGFP (Figures 2E–2G). Moreover, we saw an increase in the number of cells expressing *neurog3*:H2BGFP with all three hits (Figure 2H), indicating that the hits increased the differentiation toward the enteroendocrine lineage.

Structural diversity and specificity of the most efficient hits

The three confirmed hits, Alarelin, AZD7687, and ID-8, display large differences in size and are structurally diverse (Figures 3A–3C), supporting that they are acting via different mechanisms in agreement with them having different known targets. However, as ID-8 was the most promising in terms of decreasing glucose levels, we focused our efforts on following up on its mechanism. As ID-8 is a DYRK inhibitor, we used the *Tg*(*gip*:*nLuc*) zebrafish to perform dose-response experiments with another structurally diverse DYRK inhibitor (5-iodotubercidin [5-IT]) that was present in the screened library (Figures 3D and 3E), and compared its effect with dose-response experiments with the other hits (Figures S1H–S1J). 5-IT increased the luminescence signal, but at a higher concentration than the other hits and that used in the original screening setup.

We continued to search for more potent inhibitors beyond the screened library and found that the DYRK inhibitor AZ Dyrk1B 33 (Figure 3F) could recapitulate the effect on *Tg*(*gip*:*nLuc*) zebrafish at a lower concentration (Figure 3G). AZ Dyrk1B 33 also increased the number of K- and L-cells (Figures S2A–S2F), did not change the number of β-cells (Figures S2G–S2I), increased the number of enteroendocrine progenitor-derived K-cells (Figures S2J–S2L), and decreased glucose levels (Figure S2M). In addition to giving all the same effects as ID-8, AZ Dyrk1B 33 also increased the number of K-cells in juvenile fish compared with control-treated fish of the same size (Figures S3A–S3E). Moreover, AZ Dyrk1B 33 increased the number of Pyy-expressing enteroendocrine cells (Figures S3F–S3H).

As it was unclear which DYRK(s) mediated the effect of ID-8 (Bellmaine et al., 2017; Hasegawa et al., 2012), and 5-IT is known inhibit all DYRKs (Dirice et al., 2016), whereas AZ Dyrk1B 33 have not been tested on all DYRKs (Kettle et al., 2015), we profiled the specificity of ID-8 and AZ Dyrk1B 33 on the different DYRKs to get a better idea of which DYRKs could be responsible for the observed effects. Using *in vitro* kinase assays, we found that ID-8 inhibited DYRK1A and DYRK1B with median inhibition concentration (IC50) values in the low micromolar range, but had a modest effect on the other DYRKs (Figure 3H); AZ Dyrk1B 33 potently inhibited DYRK1A and DYRK1B with IC50 values in the low nanomolar range, inhibited DYRK2 and DYRK3 with IC50 values in the high nanomolar range, and had a modest effect on DYRK4 (Figure 3I). These results pointed to a role for DYRK1A/DYRK1B and are consistent with that the kinase domains of DYRK1A and DYRK1B are very similar, such that most inhibitors will target both these kinases to a similar degree. Thus, the inhibitor AZ Dyrk1B 33 was most potent (lowest IC50 *in vitro*) and seemed to be more useful than ID-8 as it was effective at lower concentrations in zebrafish larvae and was also effective in older fish.

Genetic silencing in GLUTag cells supports a role for Dyrk1b

DYRKs are known to phosphorylate NFAT transcription factors and thereby prohibit the shuttling of NFATs from the cytoplasm to the nucleus (Muller and Rao, 2010). Therefore, we tested whether the effect of AZ Dyrk1B 33 could be blunted by cyclosporine A and INCA6, which are two different inhibitors of the NFAT phosphatase calcineurin. Cyclosporine A binds cyclophilin and calcineurin and thereby inhibits the phosphatase activity of calcineurin, whereas INCA6 is a calcineurin-NFAT interaction inhibitor and thereby blocks NFAT dephosphorylation. Both cyclosporine A and INCA6 could blunt the effect of AZ Dyrk1B 33 in *Tg*(*gip*:*Nluc*) zebrafish larvae (Figures 4A and 4B), indicating that the NFAT pathway acts as a downstream mediator in this context.

To get an indication on whether DYRK1A or DYRK1B was the main mediator of the effects, we examined the expression of the incretins in various enteroendocrine cell lines while modulating DYRK/NFAT signaling. We found that small interfering RNA knock-down of *Dyrk1b*, but not *Dyrk1a*, stimulated *Glucagon* expression in GLUTag cells (Figure 4C). The increase in *Glucagon* expression upon *Dyrk1b* knock-down could be reversed by the calcineurin inhibitors, showing the effect of the knock-down was specific and involved NFAT-signaling (Figure 4D). We continued with examining GLP-1 expression by immunohistochemistry in the GLUTag cells and found that both ID-8 and AZ Dyrk1b 33 increased GLP-1 protein levels in

AZD7687 (B), Alarelin (C), or ID-8 (D). Gip-expressing cells were stained with α-Gip antibody. Split channels are shown in A′–D′ and A″–D″. White dashed lines outline the intestines. Scale bars, 50 μm.

(E–H) The newly generated K-cells comes from *neurog3*-expressing progenitor cells.

(E and F) Representative confocal images of *Tg*(*gip*:*TagRFP*);*Tg*(*neurog3*:*H2BGFP*) larvae treated from 3 to 6 dpf with DMSO or ID-8, displaying *gip*:*TagRFP*-expressing cells in red (E and F), *neurog3*:*H2BGFP*-expressing cells in green (E′ and F′), and overlapping *gip*:*TagRFP;neurog3*:*H2BGFP* expression in yellow (E″ and F″). Scale bars, 100 μm.

(G) Quantification of the total number of K-cells and cells co-expressing *gip*:*TagRFP* and *neurog3*:*H2BGFP* after treatment with DMSO (n = 7), AZD7687 (n = 10), Alarelin (n = 9), or ID-8 (n = 7). ****$p < 0.0001$, ****$p < 0.0001$, **$p < 0.01$.

(H) Quantification of the number of *neurog3*:*H2BGFP*-positive cells in the intestinal bulb of *Tg*(*gip*:*TagRFP*);*Tg*(*neurog3*:*H2BGFP*) after the different treatments. n = 7–12 larvae per group. **$p < 0.01$, *$p < 0.05$.

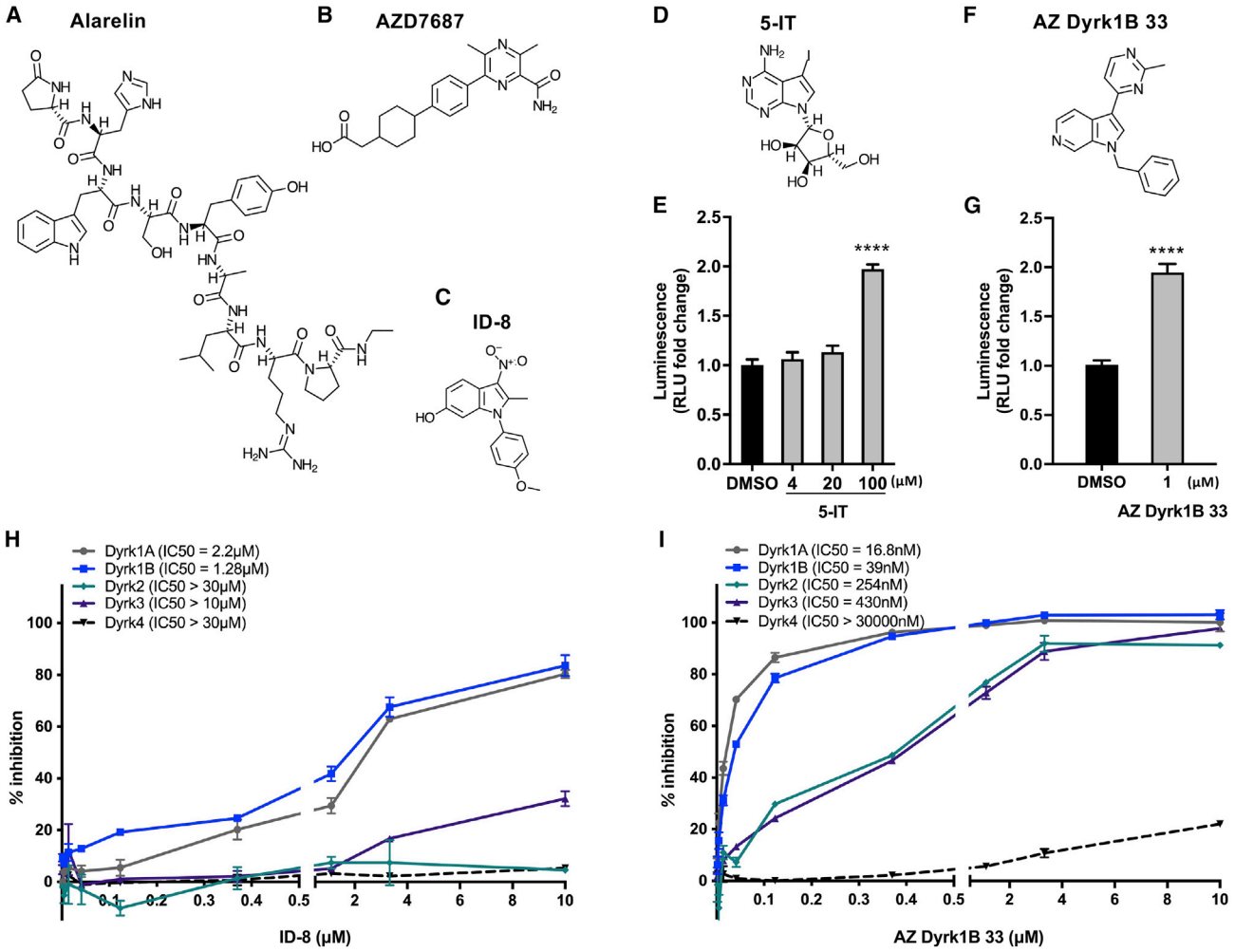

Figure 3. Structures of the hits and specificity of ID-8 and AZ Dyrk1B 33 on DYRKs

(A–C) Chemical structures of the hits. Alarelin (A), AZD7687 (B), and ID-8 (C).

(D–G) Chemical structures of the additional DYRK inhibitors followed up on, i.e., 5-IT (D) and AZ Dyrk1B 33 (F); and luminescence in *Tg*(*gip*:*Nluc*) zebrafish larvae treated from 3 to 6 days post fertilization (dpf) with 4, 20, and 100 μM 5-IT (E) or 1 μM AZ Dyrk1B 33 (G) (≥4 μM AZ Dyrk1B 33 was toxic to the zebrafish), normalized to DMSO. ****$p < 0.0001$.

(H and I) Specificity analyses of ID-8 (H) and AZ Dyrk1B 33 (I) on the DYRK-family of kinases by dose-response assessment *in vitro*. The SelectScreen biochemical kinase profiling assays were performed by ThermoFisher Scientific, using LanthaScreen for DYRK2 and Z′-LYTE for DYRK1A, DYRK1B, DYRK3, and DYRK4. See also Figure S2 and S3.

the GLUTag cells (Figures 4E–4J). Thus, this genetic approach suggests DYRK1B is the main mediator of this signaling pathway in enteroendocrine cells.

DYRK inhibitors promote enteroendocrine cell differentiation through Nfatc4

Previous work has shown the expression of NFATc1 and NFATc4 in the human intestine (Wang et al., 2011), and building on that we found that Nfatc4 expression was scattered throughout the zebrafish intestine, occasionally co-localized with *gip*:*TagRFP* (Figures 5A–5D). Therefore, we knocked down *nfatc4* with an antisense morpholino (which abolished the Nfatc4 staining) to test whether *nfatc4* was involved in the formation of K-cells (Figures 5E and 5G). Quantification of the number of *gip*-expressing cells revealed that *nfatc4*-deficient zebrafish displayed fewer *gip*-expressing cells in the intestine than the controls, whereas the number of *gip*-expressing cells in the pancreas was not decreased (Figure 5I), correlating with that we observed Nfatc4 staining in the intestine but not the pancreas (Figures 5A–5D). Treatment of control- and *nfatc4*-morpholino-injected *Tg*(*gip*:*TagRFP*) with AZ Dyrk1B 33 showed that *nfatc4* was necessary for AZ Dyrk1B 33's ability to induce K-cells (Figures 5E–5J). Thus, Nfatc4 is expressed in the intestine and loss-of-function experiments show that it is critical for the induced formation of K-cells.

AZ Dyrk1B 33 increases the prevalence of incretin$^+$ cells and improves glucose control in diabetic mice

To translate our findings to higher species and test the usefulness in a diabetes model, we examined the effect of AZ Dyrk1B

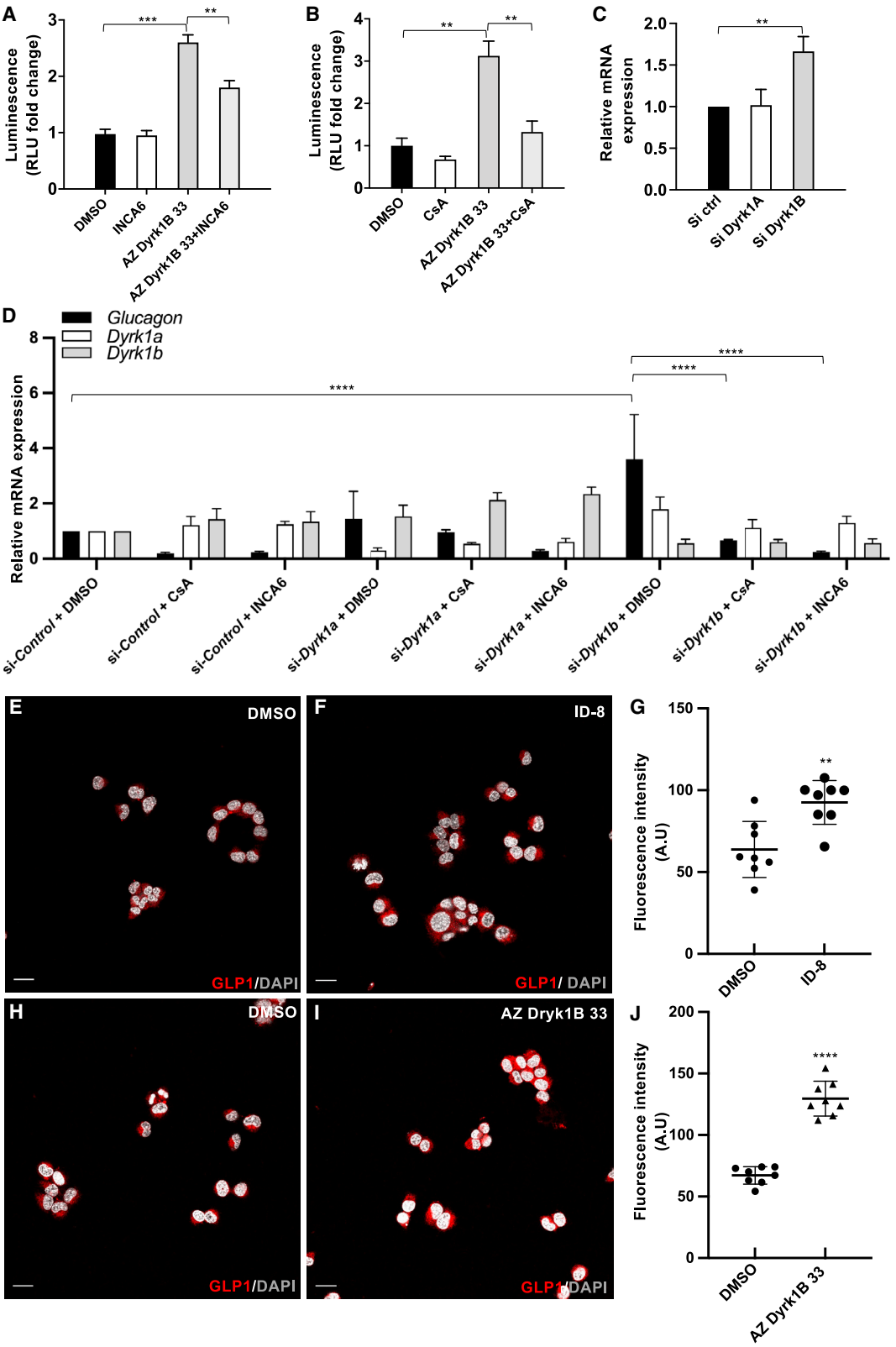

(legend on next page)

33 on diabetic mice. We used the following setup: 7-week-old diabetic *db/db* mice were orally treated for 3 weeks with vehicle or AZ Dyrk1B 33, during which time random glucose levels and body weight were monitored, and at the end of the treatment period we performed oral glucose tolerance tests (OGTT) and collected plasma and tissues (Figure S4A). The mice were not generally affected by the treatment and the body weight increased similarly in vehicle and AZ Dyrk1B 33-treated mice (Figure S4B). The random (without fasting) glucose levels were similar between the groups at the start of the study, but were significantly lower in the AZ Dyrk1B 33-treated group at the end of the treatment period (Figure S4C). Likewise, the OGTT showed that the AZ Dyrk1B 33-treated mice had an improved clearance of glucose, especially at the early time points after the administration of glucose (Figure 6A), which also resulted in a lower area under the curve during the OGTT (Figure 6B). Moreover, measurements of circulating GIP in serum showed that AZ Dyrk1B 33-treated mice displayed an enhanced response to glucose 15 min after the challenge (Figure 6C).

After the OGTT, intestines and pancreata were collected, sectioned, and used for immunohistochemistry. Expression analysis of GIP and GLP-1 showed an increased number of incretin-expressing cells in the intestines of AZ Dyrk1B 33-treated mice when compared with the control mice (Figures 6D–6G). As Dyrk1A inhibitors can stimulate proliferation of insulin-producing β-cells (Dirice et al., 2016; Wang et al., 2015), we examined sections of the pancreata from vehicle and AZ Dyrk1B 33 treated mice. Neither α- or β-cell mass (Figures 6H–6J) nor β-cell proliferation (Figures S4D–S4F) showed any difference between vehicle and AZ Dyrk1B 33-treated mice, indicating that the improved glucose tolerance with AZ Dyrk1B 33 treatment was not an effect of an altered number of β-cells. Together, these results indicate that the effect of AZ Dyrk1B 33 on incretin cell differentiation and glucose control is conserved from fish to mammals.

DISCUSSION

In this study, we performed an unbiased chemical screen for inducers of incretin-expressing cells in zebrafish. One of the identified hits inhibited DYRKs and further testing in zebrafish identified a more potent DYRK inhibitor (with a lower IC50), AZ Dyrk1B 33, that also increased incretin$^+$ cell numbers and improved glucose control in the mouse. Future studies could examine whether the effect of the DYRK inhibition on the differentiation of enteroendocrine cells is direct or systemic, e.g., by using tissue-specific genetic targeting or intestinal organoid cultures. We favor a direct effect because we found that the downstream mediator Nfatc4 was expressed in the intestine, as previously shown in the human intestine (Wang et al., 2011), and necessary for the effect of the DYRK inhibitors.

A few previous studies have used intestinal organoids to test candidates and found that, e.g., notch inhibitors (Petersen et al., 2015), Wnt inhibitors, and bone morphogenetic protein activators (Beumer et al., 2018, 2020), bile acids (Lund et al., 2020), and short chain fatty acids (Petersen et al., 2014) can stimulate enteroendocrine cell differentiation. While some of these factors affect pleiotropic signaling pathways, others are endogenous metabolites with potency in the micromolar to millimolar range, highlighting the need for potent small molecules with specific effects. Moreover, compared with organoid studies, our study offers an *in vivo* setting and high-throughput testing of diverse chemical libraries, enabling a discovery approach that is in a physiological context, as well as not testing hypotheses based on the previous literature or gene expression profiles. It would also be interesting to investigate whether the DYRK/NFAT-pathway acts upstream of enteroendocrine transcription factors regulating gastric versus intestinal enteroendocrine cell fates, such as *Neurog3* (Jenny et al., 2002) and *Nkx2.2* (Desai et al., 2008), and the recent hypothesis of predetermined specification of enteroendocrine progenitors in higher species (Bottcher et al., 2021). Interestingly, one of our hits, AZD7687, which is an inhibitor of diacylglycerol acyltransferase 1, has been shown to increase the levels of enteroendocrine hormones in a clinical trial for the treatment of type 2 diabetes and obesity (Denison et al., 2014), supporting the validity of our discovery approach in zebrafish.

We and other investigators have previously shown that compounds that either inhibit DYRK1A or decrease the expression of DYRK1A increase β-cell proliferation and function (Brial et al., 2020; Charbord et al., 2021; Dirice et al., 2016; Wang et al., 2015). However, following our treatment with AZ Dyrk1B 33 we did not see any effect on β-cell proliferation or mass, indicating that β-cell proliferation was not affecting the phenotype, although improved β-cell function may have played a role in decreasing glucose. It may be that we exposed the intestine to a greater extent than the pancreas with the oral delivery of AZ Dyrk1b 33, explaining the differential effect. In any case, it seems DYRK1A is the main regulator of β-cell proliferation (Dirice et al., 2016), and DYRK1B may be the main regulator of enteroendocrine cells, supporting the notion that the various DYRKs are important regulators of metabolic control in different tissues. In this regard, a recent study showed that DYRK1B deficiency in the liver protected mice against hepatic steatosis and insulin resistance (Bhat et al., 2022), in agreement with the idea that inhibiting DYRK1B is beneficial for metabolic control. However, there might be redundancy and species differences in which

Figure 4. Inhibition of *Dyrk1b*, but not *Dyrk1a*, promotes *Glucagon*/GLP-1 expression in a mouse enteroendocrine cell line

(A and B) AZ Dyrk1B 33 stimulates *Tg*(*gip*:*Nluc*) activity and acts via NFAT-calcineurin signaling. The effect of AZ Dyrk1B 33 (1 μM) on increasing the luminescence activity in *Tg*(*gip*:*Nluc*) transgenics can be inhibited by either 2 μM cyclosporine A (CsA) (A) or 10 μM NFAT-calcineurin association-6 (INCA6) (B). n = 4 wells per group. ***p < 0.001. **p < 0.01.

(C) Quantification of *Glucagon* expression in GLUTag cells with qPCR, after genetic silencing using control small interfering RNA (siRNA) and siRNA targeting *Dyrk1a* or *Dyrk1b*. n = 6 per group. **p < 0.01.

(D) *Glucagon* expression in GLUTag cells assessed with qPCR upon control, *Dyrk1a* or *Dyrk1b* knock-down could be reversed by either calcineurin inhibitor, i.e. CsA or INCA6. n = 3 per group. ****p < 0.0001.

(E–J) GLP-1 expression in GLUTag cells is stimulated after treatment with DYRK inhibitors. Representative confocal images of GLUTag cells stained for GLP-1 (red) and DAPI (grey) after treatment with DMSO (E, H), ID-8 (F), or AZ Dyrk1b 33 (I). Scale bars, 20 μm. Quantification of GLP-1 staining intensity per cell after treatment with ID-8 (G) or AZ Dyrk1b 33 (J) for 24 h n = 8 per group. **p < 0.01, ****p < 0.0001.

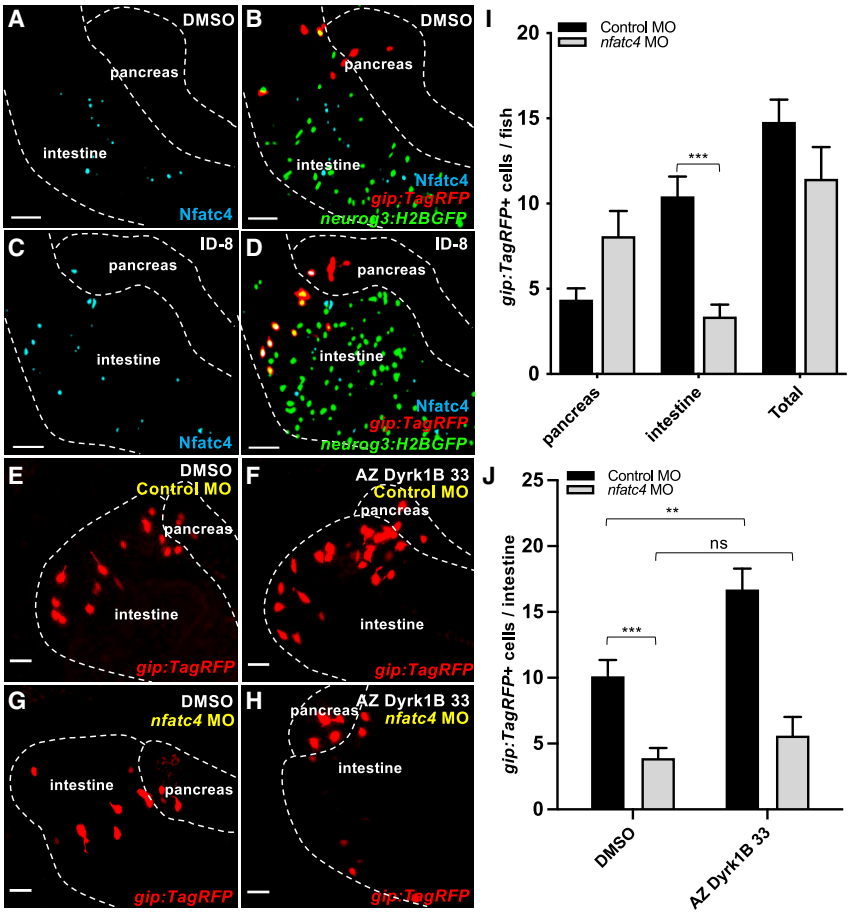

Figure 5. Nfatc4 is required for enteroendocrine cell differentiation

(A–D) Expression of Nfatc4, *gip*:*TagRFP*, and *neurog3*:*H2BGFP* in zebrafish larvae. Representative confocal images of Nfatc4 immunofluorescently stained cells, *neurog3*-expressing enteroendocrine progenitor cells, and K-cells in *Tg*(*neurog3*:*H2BGFP*);*Tg*(*gip*:*TagRFP*) zebrafish larvae treated from 3 to 6 days post fertilization (dpf) with either DMSO (A and B) or ID-8 (C and D), displaying Nfatc4 immunofluorescently stained cells in cyan blue, *neurog3*:*H2BGFP*-expressing cells in green, and *gip*:*TagRFP*-expressing cells in red. Scale bars, 50 μm.

(E–J) Knock-down *of nfatc4* decreases the number of K-cells in zebrafish intestines. (E–H) Representative confocal images of *gip*:*TagRFP*-expressing cells in 5 dpf larvae injected with control morpholinos or *nfatc4* morpholinos, and later treated with DMSO (E and G) or AZ Dyrk1B 33 (F and H) from 3 to 5 dpf, displaying *gip*:*TagRFP*-expressing cells in red. Scale bars, 20 μm.

(I) Quantification of *gip*:*TagRFP*-expressing cells in pancreas, intestines, and the total number at 5 dpf in *Tg*(*gip*:*TagRFP*) zebrafish larvae injected with control or *nfatc4* morpholinos. n = 11–14 larvae per group. ***p < 0.001.

(J) Quantification of *gip*:*TagRFP*-expressing cells in intestines of 5 dpf larvae injected with control or *nfatc4* morpholinos, and later treated with DMSO or AZ Dyrk1B 33 from 3 to 5 dpf. n = 9–10 larvae per group. ***p < 0.001, **p < 0.01.

DYRKs and NFATs are the main mediators in various tissues and cells. Future studies may expand on the specific roles of these components and which paralogs are involved in different settings and species. In this context, it is interesting to note that human *DYRK1B* gain-of-function variants have been genetically linked to the metabolic syndrome (Keramati et al., 2014), and *DYRK1B* loss-of function variants have protective effects against the metabolic syndrome (Mirshahi et al., 2014). However, it is unknown whether subjects with such variants in *DYRK1B* have affected enteroendocrine cell populations.

Developing therapeutics that increase the number of enteroendocrine cells, rather than analogs of the hormones themselves, is an attractive approach because the hormones can be secreted in a physiological manner. Although we intended to screen for incretin-expressing cells, we found that Pyy-expressing cells were also increased. In fact, increasing several enteroendocrine hormones simultaneously might be advantageous as it stimulates both the gut-to-pancreas and the gut-to-brain axes, with possible effects on both glucose control and appetite. In line with this, recent developments of dual and triple agonists have shown great promise to combat diabetes and obesity (Baggio and Drucker, 2021; Brandt et al., 2018). Interestingly, incretins from some fish species naturally act as a dual agonists and may serve as templates for development of such therapeutics (Conlon et al., 2022). Together, in this study we leverage the screening potential in zebrafish and put forward a concept in which small molecules may reinforce the enteroendocrine system, with possible implications for metabolic disease.

Limitations

This study describes a screen for small molecules increasing enteroendocrine cells in zebrafish and provides proof of concept for translating that effect from one class of hits to mice and a mouse-derived enteroendocrine cell line. However, we do not provide any evidence to whether the effect is conserved to humans, although given the distance between fish to mouse there is a good chance some hits also work in humans.

DYRK inhibitors have also been shown to increase β-cell proliferation and function. Therefore, even though we did not detect any change in β-cell proliferation or mass, increased β-cell function may have contributed to the improved glucose control. Moreover, we have not examined whether insulin secretion was increased after treatment and challenges, something that might be better studied in other models than zebrafish or *db*/*db* mice (which have high basal levels of insulin). Thus, future studies of inhibiting DYRKs in this context may extend to insulin secretion, incretin effect, various mouse models of diabetes, tissue-specific mutagenesis, and human cells and tissues. These types of possible follow-up studies are not limited to DYRK inhibitors, but apply to any interesting hit coming out from this type of phenotypic screening.

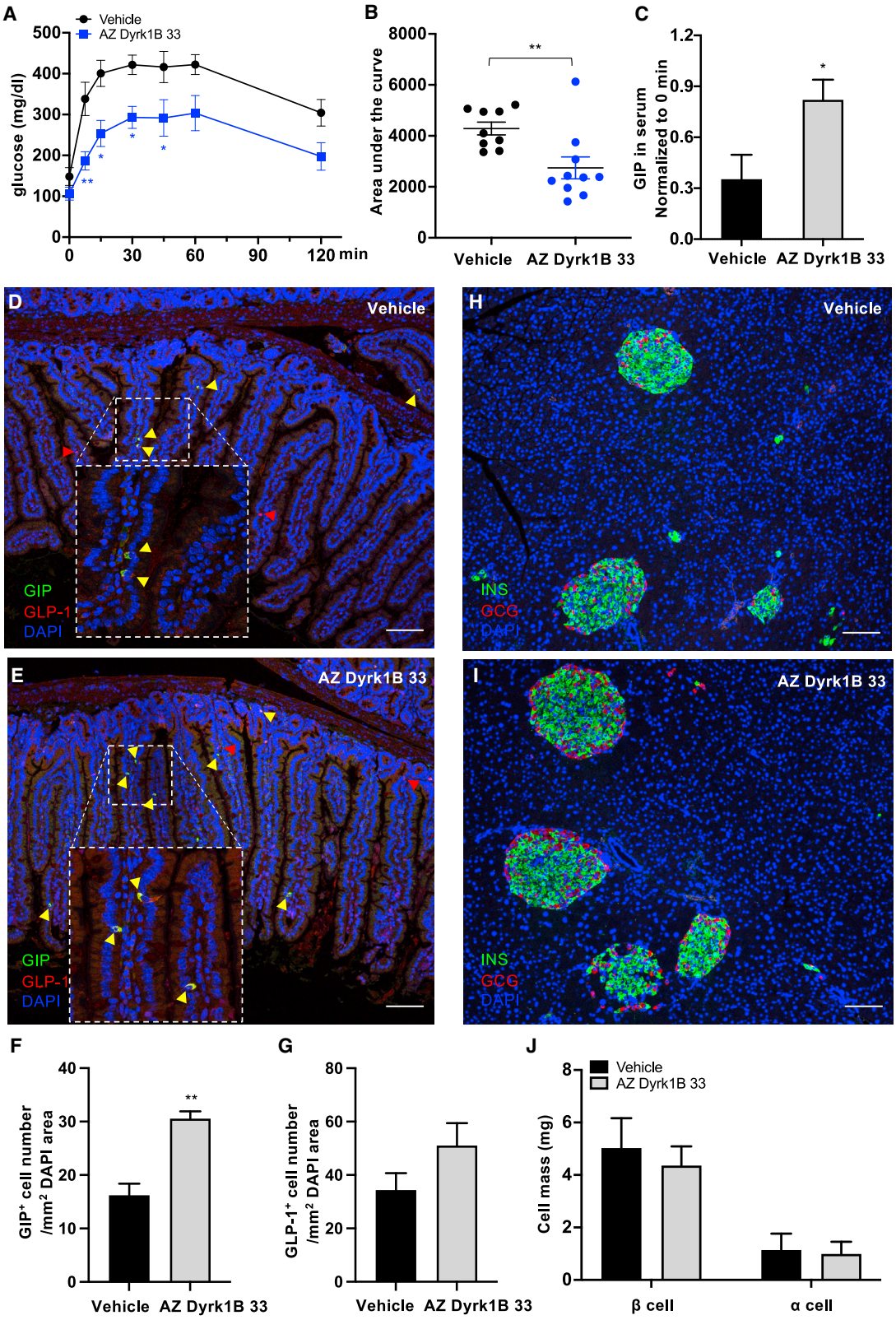

(legend on next page)

SIGNIFICANCE

The gastrointestinal tract releases hormones that have critical roles in metabolism, regulating satiety, insulin secretion, glucose levels, and more. Two of these hormones, the incretins GLP-1 and GIP, are relevant to diabetes and obesity: they are secreted by the intestine in response to food intake and enhance glucose-stimulated insulin secretion, thereby decreasing plasma glucose levels, as well as increasing satiety. To identify small molecules that increase the number of incretin-expressing cells, we established a high-throughput *in vivo* chemical screen by using the *gip* promoter to drive the expression of luciferase in zebrafish. The zebrafish model is ideal for *in vivo* drug discovery, combining the high throughput of *in vitro* screens with the physiological complexity and relevance of animal studies. We identified several hits, one of which was particularly efficient in increasing the number of incretin-expressing cells in both zebrafish and mice. However, although hits increasing the number of incretin$^+$ cells has relevance for diabetes and metabolic disease, there is a long way to clinical relevance. The phenotypic screening setup we developed may serve as a fruitful alternative to *in vitro* screens and is by no means exhausted; it can be used for screening additional chemical libraries, for which the current hits can serve as positive controls. Useful drug candidates could be those with an appropriate exposure to the gut lining but not absorbed, or quickly metabolized once absorbed, to avoid systemic effects. Overall, increasing the number of enteroendocrine cells is an understudied area that has yet to be explored therapeutically. In sum, by establishing an *in vivo* screening method, we have identified chemicals that expand the enteroendocrine cell populations, which could reinforce the gut's endogenous response to food intake and thereby improve metabolic disease.

STAR★METHODS

Detailed methods are provided in the online version of this paper and include the following:

SUPPLEMENTAL INFORMATION

Supplemental information can be found online at https://doi.org/10.1016/j.chembiol.2022.08.001.

ACKNOWLEDGMENTS

The authors thank Fiona Gribble, Frank Reimann, and Christopher Smith for input on the project; Florian Salomons for help with imaging; Etty Bachar-Wikström and Dominika Tworus for screening; Nicole Schmitner for characterizing *Tg(neurog3:H2BGFP)* founders. The graphical abstract was created with BioRender.com. This work was supported by grants to O.A. from the following sources: the Swedish Diabetes Foundation, Diabetes Wellness, Novo Nordisk Foundation, and Strategic Research Programmes in Diabetes at the Karolinska Institutet. R.N.K. was supported by NIH R01 067536 and NIH R01 129464. M.T. was supported by the EFSD/JDS Fellowship Programme.

AUTHOR CONTRIBUTIONS

L.C., M.T., C.L.M., R.T., K.L., and O.A. performed and analyzed zebrafish experiments. L.C., R.T., J.C., E.D., M.G.M., Q.Z., N.W., R.N.K., and O.A. performed and analysed translational studies. L.C. and O.A. wrote the manuscript with input from all authors. O.A. designed and conceptualized the study.

DECLARATION OF INTERESTS

The authors declare no competing interests.

Figure 6. AZ Dyrk1B 33 increases the prevalence of incretin$^+$ cells and improves glucose control in diabetic mice

(A and B) AZ Dyrk1B 33 improves the normalization of glucose during OGTT in diabetic mice.

(A) Pooled data from two OGTT experiments in BKS *db/db* mice treated by AZ Dyrk1B 33 or vehicle. The mice were fasted before the administration of glucose (0.5 mg/kg).

(B) The area under the curve for the OGTT in (A) (0–120 min). $^{**}p < 0.005$, $^{*}p < 0.05$. n = 10 AZ Dyrk1B 33-treated mice; and n = 9 vehicle-treated mice.

(C) The serum GIP level increases in AZ Dyrk1B 33-treated diabetic mice after a glucose challenge. Blood samples were collected before and at 15 min after the administration of glucose (0.5 mg/kg). GIP levels were normalized to the corresponding GIP levels in the sera sampled in the fasted state before the administration of glucose. $^{*}p < 0.05$.

(D–G) AZ Dyrk1B 33 increases the number of incretin$^+$ cells in diabetic mice.

(D and E) Representative confocal images of the small intestines of mice treated with vehicle or AZ Dyrk1B 33, displaying K-cells in green, L-cells in red, and DAPI in blue. Scale bars, 100 μm.

(F and G) Quantification of the number of GIP-expressing K-cells (F) and GLP-1-expressing L-cells (G). The total numbers of cells were normalized to the DAPI area (per mm^2). n = 4 mice per group. $^{**}p < 0.001$.

(H–J) AZ Dyrk1B 33 does not change the amount of α- or β-cells in diabetic mouse pancreata.

(H and I) Representative confocal images of the pancreata of BKS *db/db* mice treated with vehicle (H) or AZ Dyrk1B 33 (I), displaying β-cells in green, α-cells in red, and DAPI in blue. Scale bars, 100 μm.

(J) Quantification of α- and β-cell mass. n = 4 mice per group. See also Figure S4.

CellPress
OPEN ACCESS

Received: October 27, 2021
Revised: February 27, 2022
Accepted: July 27, 2022
Published: August 22, 2022

REFERENCES

Adriaenssens, A.E., Biggs, E.K., Darwish, T., Tadross, J., Sukthankar, T., Girish, M., Polex-Wolf, J., Lam, B.Y., Zvetkova, I., Pan, W., et al. (2019). Glucose-dependent insulinotropic polypeptide receptor-expressing cells in the hypothalamus regulate food intake. Cell Metab. *30*, 987–996.e6. https://doi.org/10.1016/j.cmet.2019.07.013.

Andersson, O., Adams, B.A., Yoo, D., Ellis, G.C., Gut, P., Anderson, R.M., German, M.S., and Stainier, D.Y.R. (2012). Adenosine signaling promotes regeneration of pancreatic beta cells in vivo. Cell Metab. *15*, 885–894. https://doi.org/10.1016/j.cmet.2012.04.018.

Baggio, L.L., and Drucker, D.J. (2021). Glucagon-like peptide-1 receptor co-agonists for treating metabolic disease. Mol. Metab. *46*, 101090. https://doi.org/10.1016/j.molmet.2020.101090.

Bellmaine, S.F., Ovchinnikov, D.A., Manallack, D.T., Cuddy, C.E., Elefanty, A.G., Stanley, E.G., Wolvetang, E.J., Williams, S.J., and Pera, M. (2017). Inhibition of DYRK1A disrupts neural lineage specificationin human pluripotent stem cells. Elife *6*, e24502. https://doi.org/10.7554/eLife.24502.

Beumer, J., Artegiani, B., Post, Y., Reimann, F., Gribble, F., Nguyen, T.N., Zeng, H., Van den Born, M., Van Es, J.H., and Clevers, H. (2018). Enteroendocrine cells switch hormone expression along the crypt-to-villus BMP signalling gradient. Nat. Cell Biol. *20*, 909–916. https://doi.org/10.1038/s41556-018-0143-y.

Beumer, J., Puschhof, J., Bauzá-Martinez, J., Martínez-Silgado, A., Elmentaite, R., James, K.R., Ross, A., Hendriks, D., Artegiani, B., Busslinger, G.A., et al. (2020). High-resolution mRNA and secretome atlas of human enteroendocrine cells. Cell *182*, 1062–1064. https://doi.org/10.1016/j.cell.2020.08.005.

Bhat, N., Narayanan, A., Fathzadeh, M., Kahn, M., Zhang, D., Goedeke, L., Neogi, A., Cardone, R.L., Kibbey, R.G., Fernandez-Hernando, C., et al. (2022). Dyrk1b promotes hepatic lipogenesis by bypassing canonical insulin signaling and directly activating mTORC2 in mice. J. Clin. Invest. *132*, e153724. https://doi.org/10.1172/JCI153724.

Boer, G.A., and Holst, J.J. (2020). Incretin hormones and type 2 diabetes-mechanistic insights and therapeutic approaches. Biology *9*, E473. https://doi.org/10.3390/biology9120473.

Bottcher, A., Büttner, M., Tritschler, S., Sterr, M., Aliluev, A., Oppenländer, L., Burtscher, I., Sass, S., Irmler, M., Beckers, J., et al. (2021). Non-canonical Wnt/PCP signalling regulates intestinal stem cell lineage priming towards enteroendocrine and Paneth cell fates. Nat. Cell Biol. *23*, 23–31. https://doi.org/10.1038/s41556-020-00617-2.

Brandt, S.J., Müller, T.D., DiMarchi, R.D., Tschöp, M.H., and Stemmer, K. (2018). Peptide-based multi-agonists: a new paradigm in metabolic pharmacology. J. Intern. Med. *284*, 581–602. https://doi.org/10.1111/joim.12837.

Brial, F., Alzaid, F., Sonomura, K., Kamatani, Y., Meneyrol, K., Le Lay, A., Péan, N., Hedjazi, L., Sato, T.A., Venteclef, N., et al. (2020). The natural metabolite 4-cresol improves glucose homeostasis and enhances beta-cell function. Cell Rep. *30*, 2306–2320.e5. https://doi.org/10.1016/j.celrep.2020.01.066.

Charbord, J., Ren, L., Sharma, R.B., Johansson, A., Ågren, R., Chu, L., Tworus, D., Schulz, N., Charbord, P., Stewart, A.F., et al. (2021). In vivo screen identifies a SIK inhibitor that induces beta cell proliferation through a transient UPR. Nat. Metab. *3*, 682–700. https://doi.org/10.1038/s42255-021-00391-x.

Conlon, J.M., O'Harte, F.P.M., and Flatt, P.R. (2022). Dual-agonist incretin peptides from fish with potential for obesity-related Type 2 diabetes therapy - a review. Peptides *147*, 170706. https://doi.org/10.1016/j.peptides.2021.170706.

Crosnier, C., Vargesson, N., Gschmeissner, S., Ariza-McNaughton, L., Morrison, A., and Lewis, J. (2005). Delta-Notch signalling controls commitment to a secretory fate in the zebrafish intestine. Development *132*, 1093–1104. https://doi.org/10.1242/dev.01644.

Denison, H., Nilsson, C., Löfgren, L., Himmelmann, A., Mårtensson, G., Knutsson, M., Al-Shurbaji, A., Tornqvist, H., and Eriksson, J.W. (2014). Diacylglycerol acyltransferase 1 inhibition with AZD7687 alters lipid handling and hormone secretion in the gut with intolerable side effects: a randomized clinical trial. Diabetes Obes. Metab. *16*, 334–343. https://doi.org/10.1111/dom.12221.

Desai, S., Loomis, Z., Pugh-Bernard, A., Schrunk, J., Doyle, M.J., Minic, A., McCoy, E., and Sussel, L. (2008). Nkx2.2 regulates cell fate choice in the enteroendocrine cell lineages of the intestine. Dev. Biol. *313*, 58–66. https://doi.org/10.1016/j.ydbio.2007.09.047.

Dirice, E., Walpita, D., Vetere, A., Meier, B.C., Kahraman, S., Hu, J., Dančík, V., Burns, S.M., Gilbert, T.J., Olson, D.E., et al. (2016). Inhibition of DYRK1A stimulates human beta-cell proliferation. Diabetes *65*, 1660–1671. https://doi.org/10.2337/db15-1127.

Finan, B., Müller, T.D., Clemmensen, C., Perez-Tilve, D., DiMarchi, R.D., and Tschöp, M.H. (2016). Reappraisal of GIP pharmacology for metabolic diseases. Trends Mol. Med. *22*, 359–376. https://doi.org/10.1016/j.molmed.2016.03.005.

Flasse, L.C., Stern, D.G., Pirson, J.L., Manfroid, I., Peers, B., and Voz, M.L. (2013). The bHLH transcription factor Ascl1a is essential for the specification of the intestinal secretory cells and mediates Notch signaling in the zebrafish intestine. Dev. Biol. *376*, 187–197. https://doi.org/10.1016/j.ydbio.2013.01.011.

Gasbjerg, L.S., Helsted, M.M., Hartmann, B., Jensen, M.H., Gabe, M.B.N., Sparre-Ulrich, A.H., Veedfald, S., Stensen, S., Lanng, A.R., Bergmann, N.C., et al. (2019). Separate and combined glucometabolic effects of endogenous glucose-dependent insulinotropic polypeptide and glucagon-like peptide 1 in healthy individuals. Diabetes *68*, 906–917. https://doi.org/10.2337/db18-1123.

Graham, G.V., Conlon, J.M., Abdel-Wahab, Y.H., Gault, V.A., and Flatt, P.R. (2018). Evaluation of the insulinotropic and glucose-lowering actions of zebrafish GIP in mammalian systems: evidence for involvement of the GLP-1 receptor. Peptides *100*, 182–189. https://doi.org/10.1016/j.peptides.2017.11.007.

Gribble, F.M., and Reimann, F. (2019). Function and mechanisms of enteroendocrine cells and gut hormones in metabolism. Nat. Rev. Endocrinol. *15*, 226–237. https://doi.org/10.1038/s41574-019-0168-8.

Gut, P., Reischauer, S., Stainier, D.Y.R., and Arnaout, R. (2017). Little fish, big data: zebrafish as a model for cardiovascular and metabolic disease. Physiol. Rev. *97*, 889–938. https://doi.org/10.1152/physrev.00038.2016.

Hasegawa, K., Yasuda, S.Y., Teo, J.L., Nguyen, C., McMillan, M., Hsieh, C.L., Suemori, H., Nakatsuji, N., Yamamoto, M., Miyabayashi, T., et al. (2012). Wnt signaling orchestration with a small molecule DYRK inhibitor provides long-term xeno-free human pluripotent cell expansion. Stem Cells Transl. Med. *1*, 18–28. https://doi.org/10.5966/sctm.2011-0033.

Holst, J.J., and Rosenkilde, M.M. (2020). GIP as a therapeutic target in diabetes and obesity: insight from incretin Co-agonists. J. Clin. Endocrinol. Metab. *105*, dgaa327. https://doi.org/10.1210/clinem/dgaa327.

Jenny, M., Uhl, C., Roche, C., Duluc, I., Guillermin, V., Guillemot, F., Jensen, J., Kedinger, M., and Gradwohl, G. (2002). Neurogenin3 is differentially required for endocrine cell fate specification in the intestinal and gastric epithelium. EMBO J. *21*, 6338–6347. https://doi.org/10.1093/emboj/cdf649.

Keramati, A.R., Fathzadeh, M., Go, G.W., Singh, R., Choi, M., Faramarzi, S., Mane, S., Kasaei, M., Sarajzadeh-Fard, K., Hwa, J., et al. (2014). A form of the metabolic syndrome associated with mutations in DYRK1B. N. Engl. J. Med. *370*, 1909–1919. https://doi.org/10.1056/NEJMoa1301824.

Kettle, J.G., Ballard, P., Bardelle, C., Cockerill, M., Colclough, N., Critchlow, S.E., Debreczeni, J., Fairley, G., Fillery, S., Graham, M.A., et al. (2015). Discovery and optimization of a novel series of Dyrk1B kinase inhibitors to explore a MEK resistance hypothesis. J. Med. Chem. *58*, 2834–2844. https://doi.org/10.1021/acs.jmedchem.5b00098.

Killion, E.A., Chen, M., Falsey, J.R., Sivits, G., Hager, T., Atangan, L., Helmering, J., Lee, J., Li, H., Wu, B., et al. (2020). Chronic glucose-dependent insulinotropic polypeptide receptor (GIPR) agonism desensitizes adipocyte GIPR activity mimicking functional GIPR antagonism. Nat. Commun. *11*, 4981. https://doi.org/10.1038/s41467-020-18751-8.

Kimmel, R.A., and Meyer, D. (2016). Zebrafish pancreas as a model for development and disease. Methods Cell Biol. *134*, 431–461. https://doi.org/10.1016/bs.mcb.2016.02.009.

Lam, P.Y., and Peterson, R.T. (2019). Developing zebrafish disease models for in vivo small molecule screens. Curr. Opin. Chem. Biol. *50*, 37–44. https://doi.org/10.1016/j.cbpa.2019.02.005.

Lu, J., Liu, K.C., Schulz, N., Karampelias, C., Charbord, J., Hilding, A., Rautio, L., Bertolino, P., Östenson, C.G., Brismar, K., and Andersson, O. (2016). IGFBP1 increases beta-cell regeneration by promoting alpha- to beta-cell transdifferentiation. EMBO J. *35*, 2026–2044. https://doi.org/10.15252/embj.201592903.

Lund, M.L., Sorrentino, G., Egerod, K.L., Kroone, C., Mortensen, B., Knop, F.K., Reimann, F., Gribble, F.M., Drucker, D.J., de Koning, E.J.P., et al. (2020). L-cell differentiation is induced by bile acids through GPBAR1 and paracrine GLP-1 and serotonin signaling. Diabetes *69*, 614–623. https://doi.org/10.2337/db19-0764.

Massoz, L., Dupont, M.A., and Manfroid, I. (2021). Zebra-fishing for regenerative awakening in mammals. Biomedicines *9*, 65. https://doi.org/10.3390/biomedicines9010065.

Morita, H., Komuro, I., and Carey, D.J. (2014). The metabolic syndrome and DYRK1B. N. Engl. J. Med. *371*, 785. https://doi.org/10.1056/NEJMc1408235.

Müller, M.R., and Rao, A. (2010). NFAT, immunity and cancer: a transcription factor comes of age. Nat. Rev. Immunol. *10*, 645–656. https://doi.org/10.1038/nri2818.

Musson, M.C., Jepeal, L.I., Mabray, P.D., Zhdanova, I.V., Cardoso, W.V., and Wolfe, M.M. (2009). Expression of glucose-dependent insulinotropic polypeptide in the zebrafish. Am. J. Physiol. Regul. Integr. Comp. Physiol. *297*, R1803–R1812. https://doi.org/10.1152/ajpregu.00288.2009.

Musson, M.C., Jepeal, L.I., Sharifnia, T., and Wolfe, M.M. (2010). Evolutionary conservation of glucose-dependent insulinotropic polypeptide (GIP) gene regulation and the enteroinsular axis. Regul. Pept. *164*, 97–104. https://doi.org/10.1016/j.regpep.2010.05.007.

Ng, A.N.Y., de Jong-Curtain, T.A., Mawdsley, D.J., White, S.J., Shin, J., Appel, B., Dong, P.D.S., Stainier, D.Y.R., and Heath, J.K. (2005). Formation of the digestive system in zebrafish: III. Intestinal epithelium morphogenesis. Dev. Biol. *286*, 114–135. https://doi.org/10.1016/j.ydbio.2005.07.013.

Petersen, N., Reimann, F., Bartfeld, S., Farin, H.F., Ringnalda, F.C., Vries, R.G.J., van den Brink, S., Clevers, H., Gribble, F.M., and de Koning, E.J.P. (2014). Generation of L cells in mouse and human small intestine organoids. Diabetes *63*, 410–420. https://doi.org/10.2337/db13-0991.

Petersen, N., Reimann, F., van Es, J.H., van den Berg, B.M., Kroone, C., Pais, R., Jansen, E., Clevers, H., Gribble, F.M., and de Koning, E.J.P. (2015). Targeting development of incretin-producing cells increases insulin secretion. J. Clin. Invest. *125*, 379–385. https://doi.org/10.1172/JCI75838.

Pham, D.H., Zhang, C., and Yin, C. (2017). Using zebrafish to model liver diseases-Where do we stand? Curr. Pathobiol. Rep. *5*, 207–221. https://doi.org/10.1007/s40139-017-0141-y.

Pistocchi, A., Gaudenzi, G., Foglia, E., Monteverde, S., Moreno-Fortuny, A., Pianca, A., Cossu, G., Cotelli, F., and Messina, G. (2013). Conserved and divergent functions of Nfix in skeletal muscle development during vertebrate evolution. Development *140*, 1528–1536. https://doi.org/10.1242/dev.076315.

Reuter, A.S., Stern, D., Bernard, A., Goossens, C., Lavergne, A., Flasse, L., Von Berg, V., Manfroid, I., Peers, B., and Voz, M.L. (2022). Identification of an evolutionarily conserved domain in Neurod1 favouring enteroendocrine versus goblet cell fate. PLoS Genet. *18*, e1010109. https://doi.org/10.1371/journal.pgen.1010109.

Singh, S.P., and Ninov, N. (2018). The triumvirate of beta-cell regeneration: solutions and bottlenecks to curing diabetes. Int. J. Dev. Biol. *62*, 453–464. https://doi.org/10.1387/ijdb.180067nn.

Tsuji, N., Ninov, N., Delawary, M., Osman, S., Roh, A.S., Gut, P., and Stainier, D.Y.R. (2014). Whole organism high content screening identifies stimulators of pancreatic beta-cell proliferation. PLoS One *9*, e104112. https://doi.org/10.1371/journal.pone.0104112.

Wang, P., Alvarez-Perez, J.C., Felsenfeld, D.P., Liu, H., Sivendran, S., Bender, A., Kumar, A., Sanchez, R., Scott, D.K., Garcia-Ocaña, A., and Stewart, A.F. (2015). A high-throughput chemical screen reveals that harmine-mediated inhibition of DYRK1A increases human pancreatic beta cell replication. Nat. Med. *21*, 383–388. https://doi.org/10.1038/nm.3820.

Wang, Q., Zhou, Y., Jackson, L.N., Johnson, S.M., Chow, C.W., and Evers, B.M. (2011). Nuclear factor of activated T cells (NFAT) signaling regulates PTEN expression and intestinal cell differentiation. Mol. Biol. Cell *22*, 412–420. https://doi.org/10.1091/mbc.E10-07-0598.

Xu, G., Kaneto, H., Laybutt, D.R., Duvivier-Kali, V.F., Trivedi, N., Suzuma, K., King, G.L., Weir, G.C., and Bonner-Weir, S. (2007). Downregulation of GLP-1 and GIP receptor expression by hyperglycemia: possible contribution to impaired incretin effects in diabetes. Diabetes *56*, 1551–1558. https://doi.org/10.2337/db06-1033.

Yang, B., Covington, B.A., and Chen, W. (2020). In vivo generation and regeneration of beta cells in zebrafish. Cell Regen. *9*, 9. https://doi.org/10.1186/s13619-020-00052-6.

Ye, L., Mueller, O., Bagwell, J., Bagnat, M., Liddle, R.A., and Rawls, J.F. (2019). High fat diet induces microbiota-dependent silencing of enteroendocrine cells. Elife *8*, e48479. https://doi.org/10.7554/eLife.48479.

Zecchin, E., Filippi, A., Biemar, F., Tiso, N., Pauls, S., Ellertsdottir, E., Gnügge, L., Bortolussi, M., Driever, W., and Argenton, F. (2007). Distinct delta and jagged genes control sequential segregation of pancreatic cell types from precursor pools in zebrafish. Dev. Biol. *301*, 192–204. https://doi.org/10.1016/j.ydbio.2006.09.041.

STAR★METHODS

KEY RESOURCES TABLE

REAGENT or RESOURCE	SOURCE	IDENTIFIER
Antibodies		
Chicken anti-GFP/Venus Polyclonal	Aves-Labs	Cat# GFP-1020; RRID: AB_10000240
Mouse anti-Glucagon Monoclonal	Sigma-Aldrich	Cat# G6254
Rabbit anti-Insulin Polyclonal	Cambridge Research Biochemicals	custom-made
Rabbit anti-Gip Polyclonal	Cambridge Research Biochemicals	custom-made
Rabbit anti-NFATc4 Polyclonal	Santa Cruz Biotechnology	Cat# sc-13036; RRID: AB_650208
Rabbit anti-PYY	Abcam	Cat# Ab22663; RRID: AB_2175186
Mouse anti-GIP Monoclonal	Abcam	Cat# Ab30679; RRID: AB_2109682
Rabbit anti-GLP-1 Polyclonal	Phoenix Pharmaceuticals Inc.	Cat# H-028-11
Guinea Pig anti- insulin Polyclonal	Agilent	Cat# IR00261
Rabbit anti-Ki67 Monoclonal	Abcam	Cat# Ab16667; RRID: AB_302459
Alexa Fluor secondary antibodies	Life Technologies	As specified
Chemicals, peptides, and recombinant proteins		
Compound screening Library	MedChemExpress	HY-L001 Bioactive Compound Library
PTU	Alfa Aesar	Cat# 10167220
ID-8	MedChemExpress	Cat# HY-15838
ID-8	Selleckchem	Cat# S7327
ID-8	APExBIO	Cat# B1952-50
Alarelin	MedChemExpress	Cat# HY-17405
AZD7687	MedChemExpress	Cat# HY-15497
AZ Dyrk1B 33	Bio-techne TOCRIS	Cat# 5632
5-IT	Merck	Cat# 24386934
INCA6	MedChemExpress	Cat# HY-108544
Cyclosporine A	MedChemExpress	Cat# HY-B0579
Metronidazole	Sigma-Aldrich	Cat# M1547
DMSO	Fisher Scientific	Cat# AA36480AP
EdU (5-ethynyl-2'-deoxyuridine)	Invitrogen	Cat# E10187
DAPI (4′,6-Diamidino-2-Phenylindole, Dihydrochloride)	Invitrogen	Cat# D1306
Hydroxypropylmethylcellulose	Sigma-Aldrich	Cat# H9262
Tween80	Sigma-Aldrich	Cat# P1754
Formaldehyde 4% stabilised, buffered (pH 7.0 ± 0.2)	VWR	Cat# 9713.5000
Target Retrieval Solution, Citrate pH 6	Dako	Cat# S236984
DPP-IV inhibitor	Sigma-Aldrich	Cat# DPP4
Triton X-100	Merck	Cat# X100-500ML
PBS	ThermoFisher SCIENTIFIC	Cat# 70011–036
BSA	Sigma-Aldrich	Cat# A4503-100G
NaN3	Sigma-Aldrich	Cat# S2002-5G
Hepes Buffer Solution	Gibco	Cat# 15630-056
Fetal bovine serum (FBS)	Gibco	Cat# 16140071
Dulbecco's modified Eagle's medium (DMEM)	Gibco	Cat# 10569010
Penicillin-Streptomycin	Gibco	Cat# 10378016
Dharmafect 1 siRNA transfection reagent	Dharmacon	Cat# T-2001-03

(*Continued on next page*)

Continued

REAGENT or RESOURCE	SOURCE	IDENTIFIER
iTaq Universal SYBRGreen Supermix	BioRad	Cat# 1725124
Critical commercial assays		
Glucose Colorimetric/Fluorometric Assay Kit	Biovision	Cat# K606
Nano-Glo™ Luciferase Assay System	Promega	Cat# N1110
Click-iT™ EdU Cell Proliferation Kit for Imaging, Alexa Fluor™ 647 dye	Invitrogen	Cat# C10340
New Mouse GIP Enzyme-linked immunosorbent assay Kit	Crystal Chem	Cat# 81527
RNeasy-Kit	QIAGEN	Cat# 74004
Superscript II one-step RT-PCR system	Invitrogen	N/A
Experimental models: Organisms/strains		
Zebrafish: AB strain	ZIRC	ZFIN: ZDB-GENO-960809-7
Zebrafish: *Tg(gcga:GFP)*^{ia1}	(Zecchin et al., 2007)	ZFIN: DB-TGCONSTRCT-070215-2
Zebrafish: *Tg(ins:H2BGFP;ins:dsRed)*^{s960}	(Tsuji et al., 2014)	ZFIN: ZDB-ALT-131001-6
Zebrafish: *Tg(gip:Venus)*^{KI121}	This manuscript	N/A
Zebrafish: *Tg(gip:Nluc)*^{KI122}	This manuscript	N/A
Zebrafish: *Tg(gip:TagRFP)*^{KI123}	This manuscript	N/A
Zebrafish: *Tg(neurog3:H2BGFP)*^{KI124}	This manuscript	N/A
C57BLKS Leprdb homozygous mice	Janvier	JAX: 000697; RRID: IMSR_JAX:000697
Oligonucleotides		
Morpholino oligonucleotide *nfatc4*: see Table S1	Gene Tools	(Pistocchi et al., 2013)
Morpholino oligonucleotide control	Gene Tools	PCO-StandardControl-100
Primers for cloning zebrafish promoters *gip*: see Table S1	This manuscript	N/A
Primers for cloning zebrafish promoters *neurog3*: see Table S1	This manuscript	N/A
Primers for mouse *Gcg*: see Table S1	This manuscript	N/A
Primers for mouse *Tbp*: see Table S1	This manuscript	N/A
Primers for mouse *Dyrk1a*: see Table S1	This manuscript	N/A
Primers for mouse *Dyrk1b*: see Table S1	This manuscript	N/A
Recombinant DNA		
pENTR/TEV/D-TOPO	ThermoFisher SCIENTIFIC	K252520
Software and algorithms		
Fiji/ImageJ	Open source	https://imagej.net/Fiji
GraphPad PRISM 9.1.2	GraphPad Software, Inc	https://www.graphpad.com/
Excel	Microsoft	https://www.microsoft.com/en-us/microsoft-365?rtc=1

RESOURCE AVAILABILITY

Lead contact

Further information and requests for resources and reagents should be directed to and will be fulfilled by the lead contact, Olov Andersson (olov.andersson@ki.se).

Materials availability

There are restrictions to the availability of the custom-made antibodies used in this study. The custom-made antibodies against Insulin and Gip were generated by Cambridge Research Biochemicals. We are glad to share the antibodies with reasonable compensation by requestor for its processing and shipping.

Zebrafish lines generated in this study will be made available for academic purposes upon request; commercial applications might require a contract and/or a completed Materials Transfer Agreement.

Data and code availability

All data reported in this paper will be shared by the lead contact upon request. The paper does not report original code. Any additional information required to reanalyze the data reported in this paper is available from the lead contact upon request.

EXPERIMENTAL MODEL AND SUBJECT DETAILS

All animal experiments were conducted at the Solna campus, Karolinska Institutet (Stockholm, Sweden). All procedures were performed in accordance with the Swedish and European Union guidelines and regulations under ethical permits approved by Stockholms Norra Djurförsöksetiska Nämnd.

Zebrafish

Zebrafish were group-housed in standardized water tanks at 28°C and with a 14:10 h light:dark cycle. Wild type zebrafish were of the AB strain. The following previously reported transgenic zebrafish lines were used: *Tg(ins:H2BGFP;ins:dsRed)*^{s960} (Tsuji et al., 2014), and *Tg(gcga:GFP)*^{ia1} (Zecchin et al., 2007). In this manuscript, we generated *Tg(gip:Venus)*^{KI121}, *Tg(gip:Nluc)*^{KI122}, *Tg(gip:TagRFP)*^{KI123} and *Tg(neurog3:H2BGFP)*^{KI124} zebrafish lines within the background of the AB strain. All transgenic zebrafish were healthy and fertile. Larvae and juvenile zebrafish without sex determination were chosen for experiments randomly. Adult zebrafish were fed dry food twice per day, while larval and juvenile zebrafish were additionally fed live artemia 4 times per week.

BKS db/db mice

BKS db/db mice (B6.BKS(D)-Lepr^{db}/J) were purchased from Janiver, but initially from JAX (Strain #:000697). Mice were group-housed in standardized cages with 12:12 h light:dark cycle and with unlimited access to regular chow diet except during the fasting period. Water was provided all the time. The mice became obese at 3 to 4 weeks of age with elevations of blood sugar at four to eight weeks. Male mice were between 28 to 40 grams in weight, and the random blood glucose levels were between 216 to 450 mg/dL at study initiation. Either vehicle or compounds were administered to the mice through oral gavage every day from 7 to 10 weeks of age. We measured the starting body weight (BW) and random glucose (RG) level at 6 weeks and 6 days of age, followed by 8 h of fasting. The fasting body weight and glucose (FG) were recorded. The change in the glucose levels from before to after fasting and the original body weight were used to match the mice into equal groups prior to either vehicle or drug treatment.

GLUTag cell line

A murine enteroendocrine cell line, GLUTag cells, were purchased from ATCC and cultured in Dulbecco's modified Eagle's medium (DMEM) containing 4.5 g/L glucose, 10% fetal bovine serum (FBS), and 1× Penicillin-Streptomycin solution, and maintained at 37 °C and 5% CO2.

METHOD DETAILS

Zebrafish experimental procedures

Cloning

The *gip* transgenic lines were generated by cloning 1188 bp of the proximal promoter (starting directly upstream of the ATG) of *gip* into the plasmid pENTR/TEV/D-TOPO by using primers FWD: 5′-TTTTTTCCCTCCCCGTAATACTTC-3′ and REV: 5′-CACCCG CAGCCTCGAGGTAAAATA-3′, followed by LR cloning of the *gip* promoter upstream of Venus in a destination vector, resulting in *Tg(gip:Venus)*^{KI121}. To generate *Tg(gip:Nluc)*^{KI122} and *Tg(gip:TagRFP)*^{KI123} zebrafish, the *Nluc* and *TagRFP* inserts were amplified and placed downstream of the *gip* promoter by replacing *Venus* in the *gip:Venus* plasmid via restriction enzyme digestion and in-fusion cloning.

The *Tg(neurog3:H2BGFP)*^{KI124} was generated by cloning 2111 bp of the proximal promoter (starting directly upstream of the ATG) of *neurog3* by using primers FWD: 5′-CACCCATTCACTGCAGCACCAAAG-3′ and REV: 5′-TCTGTACTGAAAAACACAACGAG-3′ into the plasmid pENTR/TEV/D-TOPO, followed by LR cloning of the *neurog3* promoter upstream of H2BGFP in a destination vector.

Chemical screening

Tg(gip:Nluc) fish were crossed with wild-type fish to assess the effects of the compounds. Three 3 dpf zebrafish larvae per well in 96-well plates were incubated in 200 μL E3 + PTU medium containing either 1% DMSO or 20 μM chemicals from the library (MedChemExpress), which was dissolved in DMSO. After three days of treatment, 50 μL mixture of Nano-Glo™ Luciferase Assay Buffer and Substrate (Promega) was added to each well and incubated for 2 h at room temperature. By the end of incubation, the luminescence signals were detected by a Glomax-96 microplate luminometer (Promega). For each clutch, at least 8 wells were treated with DMSO and their average value of luminescence were used to normalize the luminescence values from other wells belonging to the same clutch. The effect of the compounds was assessed by the calculation of Z-scores: Z-score=(Luminescence value (compound-treated wells)-Average Luminescence value (DMSO-treated wells)) / Standard Deviation (DMSO-treated wells). Compounds with a Z-score > 2 were considered to be positive and selected as primary hits. All the primary hits were retested in an additional 4 wells to enable the selection of secondary hits. The final hits were selected after testing potential secondary

hits for up to 10 wells. Both the average Z-score and the frequency of positive results for each hit were used for determining the final hits.

Glucose assay in zebrafish

To investigate the glucose levels in zebrafish larvae we measure free glucose, i.e., essentially extracellular glucose as intracellularly glucose is phosphorylated by hexokinases (thereby we use free glucose as an estimate of glycemia). Wild-type zebrafish larvae were randomly grouped and treated from 3 to 6 dpf, and then left for a one-day washout to 7 dpf. The glucose levels were detected by lysing 16 zebrafish larvae (2 larvae were pooled per data point) from the control and treated groups. Snap frozen larvae were analyzed as previously described (Andersson et al., 2012). In brief, 25 μL PBS were added to each larvae sample. The larvae were lysed with a tissue lyser (TissueLyser II, QIAGEN) for 2 min at a frequency of 20/s. Then, lysed tissues were centrifuged for 5 min at 12000 rpm, and 5 μL of the supernatant were used for glucose assay according to the protocol provided by the Glucose Colorimetric/Fluorometric Assay kit (Biovision).

Immunofluorescence and EdU staining of zebrafish

Immunostaining and 5-Ethynyl-2′-deoxyuridine (EdU; Invitrogen) staining were performed on larvae according to our previous report (Lu et al., 2016) and manufacturers' protocols. Briefly, after 3 days of treatment, zebrafish larvae were washed three times in H2O and fixed with 4% formaldehyde overnight at 4 °C. Fixed larvae were washed three times with PBS, and the zebrafish skin were removed with forceps. The larvae were incubated in blocking buffer (PBS, 0.3% Triton X-100, 4% BSA, and 0.02% NaN3) at room temperature for at least 2 h before addition of the primary antibodies and further incubation overnight at 4 °C. After the primary antibodies were removed, the larvae were wash with PT buffer (PBS and 0.3% Triton X-100) eight times for at least 2 h at room temperature. DAPI at 1:1000 (D1306, 5 g/mL, Invitrogen) and Alexa Fluor secondary antibodies at 1:500 (Life Technologies) were diluted with blocking buffer, added to the larvae, and incubated overnight at 4 °C. Then, the larvae were washed with PT buffer eight times for at least 2 h at room temperature before mounting for imaging. The Chicken anti-GFP primary antibody was used to amplify the signal of GFP/Venus at 1:500 (GFP-1020, Aves Laboratories), the Rabbit anti-Gip antibody was used to detect Gip in zebrafish at 1:200 (customized, Cambridge Research Biochemicals), the Rabbit anti-PYY antibody was used to detect the expression of zebrafish peptide YY at 1:100 (Ab22663, Abcam), and the Rabbit anti-Nfatc4 antibody was used to detect the expression of Nfatc4 in zebrafish at 1:50 (sc-13036, Santa Cruz Biotechnology). Cell proliferation was assessed by adding 10 mM EdU to E3 media containing 10 mM Hepes, i.e. prior to treatment of the larvae. After staining with secondary antibodies, EdU incorporation was detected with the Click-iT EdU Alexa Fluor 647 imaging kit (Invitrogen) according to the manufacturere's protocol.

Juvenile zebrafish were treated with either DMSO or the compounds for 3 or 7 days, and the solutions were refreshed every day. Fixation was performed overnight at 4°C. Before being mounted for imaging, the skin and muscles were removed.

Knock-down of nfatc4 in zebrafish

Knock-down of *nfatc4* was performed by injecting *Tg(gip:TagRFP)* zebrafish embryos at the one-cell-stage with 8 ng of a morpholino targeting the first intron-exon splice junction of *nfatc4*, (5′-3′) CAGGAAAATGTGCTTCCCACCTGTA (Gene Tools) (Pistocchi et al., 2013). The standard control morpholino (5′-3′) CCTCTTACCTCAGTTACAATTTATA (Gene Tools) was used as reference. MO-injected embryos were also treated with DMSO or AZ Dyrk1B 33 from 3 to 5 dpf to determine the requirement of *nfatc4* for the effect of AZ Dyrk1B 33.

Mouse experimental details

In vivo *mouse study*

Either vehicle or AZ Dyrk1B 33 (10 mg/kg) were administered to the mice through oral gavage. The vehicle solution consisted of 0.5% hydroxypropylmethylcellulose and 0.1% Tween80 in PBS, and AZ Dyrk1B 33 was suspended in the vehicle solution. Random glucose levels and body weight were monitored according to the timeline in Figure S4A. By the end of the treatment, mice were fasted and OGTT was performed, after which the mice were sacrificed. Pancreata and intestines were fixed in 4% formaldehyde overnight at 4 °C. After being embedded in paraffin, tissues were sectioned. Sections from the middle levels were chosen for deparaffinization and antigen retrieval with citrate buffer pH 6 (S236984, Dako). Then sections were stained overnight at 4 °C with the following primary antibodies: anti-GIP at 1:250 (Ab30679, Abcam), anti-GLP-1 at 1:250 (H-028-11, Phoenix Pharmaceuticals Inc.), anti-insulin at 1:2 (IR00261, Agilent), anti-Ki67 at 1:250 (ab16667, Abcam) and anti-glucagon at 1:200 (G2654, Sigma-Aldrich). The sections were then washed and incubated for two hours with Alexa Fluor secondary antibodies at 1:500 (Life Technologies) and DAPI 5 g/mL at 1:1000 (D1306, Life Technologies) before imaging with an ImageXpress Pico microscope -(Molecular Devices), Zeiss LSM980-Airy, or a Leica SP8 confocal microscope. Quantification of the number of cells and the area were analyzed with ImageJ, and cell mass was calculated by multiplying the fraction of cell area with the weight of the whole pancreas.

Glucose tolerance test

Mice were fasted overnight, and then 0.5 g glucose/kg body weight were administered orally by gavage. Blood glucose levels were measured at 0, 7.5, 15, 30, 45, 60 and 120 min after the administration of glucose.

Measurement of serum parameters

Blood samples were collected in EDTA-coated tubes, and then 20 μL DPP-IV inhibitor was added into the samples before they were centrifuged for 10 min at 12,000 rpm. The supernatants were collected for further Enzyme-linked immunosorbent assays (ELISA) for determining GIP levels with an ELISA kit (81527, Crystal Chem).

Cell culture experimental details

Chemical inhibition of DYRKs in GLUTag cells was achieved through treatment with ID-8 or AZ Dyrk1B 33 over 24 h, at the concentration of 10 μM and 1 μM, respectively. Alternatively, GLUTag cells were seeded into 6-well culture plates at 2.5×10^6 cells per well. After 24 h of culture, cells were transfected over 24 h with one of two different siRNA against *Dyrk1a* (MSS203739 from Invitrogen was used in Figure 4, and the effects were validated with MSS203740 from Invitrogen) and *Dyrk1b* (AM16704 from Ambion was used in Figure 4, and the effects were validated with MSS203742 from Invitrogen) at the concentration of 20 nM, using Dharmafect 1 siRNA transfection reagent (Dharmacon) according to the manufacturer's protocol.

RNA isolation and reverse transcription were performed using RNeasy-Kit (Qiagen) and Superscript II one-step RT-PCR system (Invitrogen), respectively. Real-time PCR analyses were carried out on a ViiA7 (Thermo Fisher Scientific) using SYBR-Green (BioRad), and the result of each sample was normalized to *Tbp*. Primer sequences are provided in the Table S1.

For immunofluorescence staining of GLUTag cells, the cells were grown and treated on glass coverslips, then fixed with 4% PFA for 10 minutes at room temperature. Following fixation, the cells were permeabilized with PBS-Triton 0.05% and then blocked in PBS with 3% BSA for 1 h at room temperature and incubated with primary antibodies overnight at 4 °C (anti-GLP-1, H-028-11, Phoenix Pharmaceuticals), then with appropriate secondary antibodies conjugated with Alexa 555 red (Invitrogen). Cells were counterstained with DAPI (Vectashield) for 20 minutes and visualized by confocal microscopy (Leica SP8). We then used the Fiji software to quantify the expression level of GLP-1. Each value describes the fluorescence intensity (Arbitrary unit) divided by the number of cells within the same field of view.

QUANTIFICATION AND STATISTICAL ANALYSIS

The exact number of biological replicates (n) are described in figure legends. Values were expressed as mean ± SEM. Statistical analyses were performed by unpaired t-tests when two groups were analyzed, and One-way or Two-way analysis of variance (ANOVA) followed by a Tukey's post hoc test using GraphPad PRISM version 9.1.2 software (GraphPad Software, La Jolla, CA, USA) when more than two groups were analyzed. The significance level was defined as $p < 0.05$. No data were excluded. The investigators were generally not blinded. All experiments were repeated at least two times, with the majority of them having more than three biological replicates, and were reproducible. The zebrafish larvae were randomly assigned to the respective treatment groups whereas the mice were stratified into groups prior to treatment, as described in the STAR Methods.